Microhardness Variations in HSLA-100 Welds Fabricated with New Ultra-Low-Carbon Weld Consumables

HSLA-100 steel weldments made with ultra-low-carbon consumables were investigated by TEM and microhardness mapping analyses

BY D. W. MOON, R. W. FONDA AND G. SPANOS

ABSTRACT. Microstructural evolution resulting from gas metal arc welding of HSLA-100 steel plate with an experimental ultra-low-carbon weld consumable, designated CTC-03, was investigated by transmission electron microscopy, optical microscopy and microhardness analyses. A color microhardness map was generated from more than 1600 diamond indentation measurements taken across the transverse cross section of the weldment, to make a direct correlation between the microhardness variations and the corresponding microstructures. Eight characteristic areas of the CTC-03/HSLA-100 weld were selected to study the corresponding microstructure by TEM and optical microscopy, and the microstructures were then correlated with the microhardness map. The microstructure throughout the fusion zone (FZ) consists of a majority of lath ferrite with varying amounts (depending on the location) of untempered fine-lath martensite, some interlath retained austenite, and spherical oxide inclusions. The softest regions of the fusion zone are in curved white bands located at the lower portions of the heat-affected zones of the weld beads. The microstructure within these white bands is predominantly lath ferrite. The hardest regions in the fusion zone are located between the bead boundaries and these white bands, and contain significant amounts of fine untempered lath martensite. The base plate heat-affected zone (HAZ) consists of a mixture of untempered lath martensite and coarse autotempered plate martensite. The as-received HSLA-100 base metal exhibits a quench-and-tempered microstructure with a majority of fine-lath martensite and significant amounts of coarse martensite. Despite its low heat input, the CTC-03 weldment exhibits hardness values comparable with those of the HSLA-100 base metal and similar to some weldments made with other filler metals. The microhardness map of this weld was compared to four other microhardness maps developed for welds made with other candidate ULC filler metals and/or different heat inputs. In all five weldments studied, the midsection of the HAZ of the base metal (*i.e.,* the region located about midway between the weld interface and the outer boundary of the HAZ) is the hardest region of the weld, regardless of base metal, filler metal type or heat input.

D. W. MOON, R. W. FONDA and G. SPANOS are with the Naval Research Laboratory, Washington, D.C.

Introduction

The family of high yield (HY) strength steels, including HY-80, HY-100 and HY-130, has been extensively used by the U.S. Navy since its development in 1946 (Ref. 1). The strength and toughness of these steels are derived from the formation of quenched and tempered martensite. While carbon plays a major role in the strengthening mechanism of these steels through the formation of fine dispersions of carbides, it can also promote the formation of deleterious untempered martensite microstructures during fast cooling. These deleterious microstructures have an enhanced susceptibility to hydrogen-assisted cracking (Ref. 2). Thus, welding of these steels requires strict control of the heat input and preheat/interpass temperature to ensure the production of acceptable microstructures and mechanical properties. Since these constraints on the welding operational envelope are very costly, the U.S. Navy has pursued, since about 1980, high-strength low-alloy (HSLA) steels as a replacement for HY steels.

HSLA steels are lower carbon, copper-precipitation-strengthened steels that meet the strength and toughness requirements of HY steels, yet are more easily welded without preheat. Use of these HSLA steels in surface ship and submarine construction can result in significant reductions in production costs through the minimization or elimination of preheat, utilization of a wider range of energy inputs and employment of more relaxed fabrication control (Refs. 3–7). However, welding consumables that take full advantage of the benefits of HSLA base metal have yet to be developed, certified and put into production (Refs. 1, 5). Welding consumables originally designed for HY-steels are currently being used to weld HSLA steels for limited ap-

KEY WORDS

HSLA-100
Microhardness
Ultra-Low Carbon
High-Strength Steel
Naval Ships
Filler Metal
Hydrogen Cracking

plications in naval ships, but when made without preheat these weldments have been found to be susceptible to hydrogen-assisted cracking. Therefore, the Navy has been spearheading the development of new welding filler metals for welding both HSLA and HY steels (Ref. 6). The aim of this program is to develop new welding consumables that can be welded with 1) no preheat or no interpass temperature controls when welding thick HSLA steel plates, 2) reduced costs for inspection and hydrogen damage controls and 3) reduced preheat/interpass temperatures and heat input controls, including elimination of postweld soak, during welding of HY-100 base plate (Ref. 6).

The major design concept in developing these new consumables is to significantly reduce the carbon content. These alloys are therefore referred to as ultra-low-carbon (ULC) (Ref. 5) or ultra-low-carbon-bainitic (ULCB) consumables (Refs. 1, 5). The loss in strength due to the carbon reduction is at least partially offset by judiciously increasing the Mn, Mo and Ni concentrations (Ref. 8). Using such a welding consumable could widen the welding process window and reduce the Navy's shipbuilding cost by millions of dollars (Ref. 9). The fine scale of the microstructures present in these ULC steels cannot be adequately resolved by optical microscopy to characterize and differentiate the different microconstituents. Thus, higher-resolution techniques such as transmission electron microscopy (TEM) must be used. Only a limited number of studies have employed TEM to characterize the microstructures in welds made with these new ULC filler metals, *e. g.*, Refs. 10–13. The majority of investigations have used optical microscopy to correlate the weld microstructures with their mechanical properties.

In order for the Navy (and industry) to develop, certify and employ advanced ULC filler metals in ship and submarine construction, it is essential that the microstructural and property evolution throughout these new ULC weldments be well understood. This type of knowledge is critical in developing weld metals and welding procedures that minimize both cost and the potential factors for failure, yet provide for equivalent or enhanced final properties. Therefore, the aim of the present study is to determine the microstructural evolution and microstructure-microhardness correlations throughout the fusion zone and the HAZ of an HSLA-100 weldment made using an experimental ULC filler metal, designated CTC-03. In addition, direct comparisons are made between the color microhardness map developed for the current weld and those for welds made with different filler metals, base metals and heat inputs.

Experimental Procedure

Using an exploratory ultra-low-carbon Mn-Ni-Mo weld consumable, CTC-03, 1-in.-thick HSLA-100 steel plates were welded by the National Center for Excellence in Metalworking Technology (NCEMT). The CTC-03 weld consumable was developed by the NCEMT under its Navy Manufacturing Technology program (Ref. 14). The multipass GMA welding process employed a single-V joint configuration with a 45-deg included angle. A backing plate of the same HSLA-100 base plate was used beneath the root. This weldment, CTC-03D, was fabricated in the spray transfer mode with a heat input of 30 kJ/in. (1200 kJ/m), a 16 in./min (41 cm/min) welding speed, a 125°F (52°C) preheat temperature and a 125°F interpass temperature. For further details of the welding procedure, see Ref. 14. The chemical compositions of the base metal, the welding consumable and the as-deposited weld metal are shown below in Table 1. The mechanical properties of the HSLA-100 base plate are 113 ksi (779 MPa) yield strength (YS), 127 ksi (876 MPa) ultimate tensile strength (UTS), 22% elongation (El), 71% reduction in area (RA) and 91 ft-lb (123 J) CVN impact toughness at –120°F (–84°C) (Ref. 8). The average mechanical properties taken from the center of the as-deposited weld metal of the CTC-03D weld (the D designates the 30 kJ/in. heat input) are 114 ksi (786 MPa) YS, 119.2 ksi (822 MPa) UTS, 19.3% El, 63.3% RA and a CVN impact toughness of 124 ft-lb (168 J) at 0°F (–18°C) and 86 ft-lb (117 J) at –60°F (–51°C) (Ref. 14).

All microstructural observations were taken from transverse cross sections from the weldment. These cross sections included the fusion zone, the heat-affected zone and the unaffected base metal — Fig. 1A. After coarse polishing with successively finer grit papers, weld cross sections were polished first with 3-µm and 1-µm diamond paste, and then with a 0.06-µm silica suspension. They were subsequently etched with a solution of picric acid saturated in 100 mL of water with 10 g of sodium tridecylbenzene sulfonate (Ref. 15) to reveal the weld solidification structure. To study the solid-state microstructure for optical microscopy a 1% nital etchant was used. Microhardness maps across the base metal, heat-affected zone and fusion zone were developed using a diamond indentor with a 1-kg load. After polishing away the etched sur-

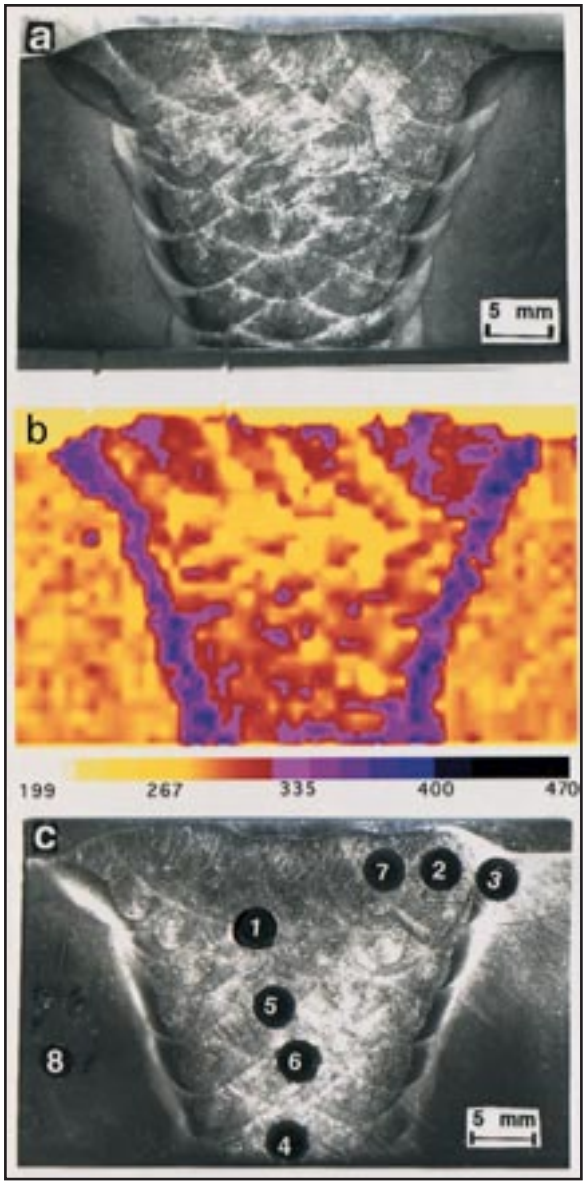

Fig. 1 — Transverse cross section of the CTC-03D weldment. A — Macrograph; B — microhardness map; C — macrograph with the selected areas for TEM and optical microscopy studies circled.

Table 1 — Compositions of Base Metals, Welding Consumable and As-Deposited Weld Metal (wt-%)

	C	Ni	Mn	Mo	Cu	Cr	Si	Al	Ti	P	S	V	Nb	Zr
HY80 base plate (a) (welded w/ARC100)	0.16	2.49	0.30	0.43	0.016	1.39	0.25			0.010	0.004	0.004		
HSLA100 base plate (b) (welded w/CTC03 and CTC08)	0.055	3.41	0.81	0.57	1.53	0.73	0.22	0.009	0.008	0.07	0.001	0.0011	0.032	
HSLA100 base plate (a) (welded w/ARC100)	0.035	3.14	0.79	0.57	1.37	0.57	0.22	0.027		0.004	0.001		0.028	
CTC03 consumable (d)	0.028	3.78	1.54	0.52	0.001	0.01	0.34		0.028	0.001	0.002	0.001		
CTC03D weld metal (c)	0.035	3.72	1.42	0.46	0.09	0.09	0.33	0.006	0.014	0.008	0.002	0.005		
CTC08 consumable (d)	0.03	3.72	1.80	0.99	0.001	0.01	0.33		0.025	0.001	0.002	0.003		
CTC08A weld metal (e)	0.040	3.70	1.56	0.89	0.08	0.06	0.30		0.013			0.005	0.014	
CTC08C weld metal (e)	0.053	3.70	1.5	0.83	0.34	0.16	0.27		0.009			0.005	0.015	
ARC100 consumable (f)	0.018	2.67	1.63	0.46	0.001	0.01	0.29	0.002	0.006	0.003	0.001	0.005		0.002
ARC100 weld metal (f)	0.025	2.72	1.40	0.47	0.067	0.05	0.26	0.004	0.004	0.003	0.001	0.009		0.001

The chemical compositions of (a) and (b) were determined ny NLR, (c) by Ref. 14, (d) by VIM ingots (Ref. 23), (e) by Ref. 23 and (f) by Electric Boat Corp.

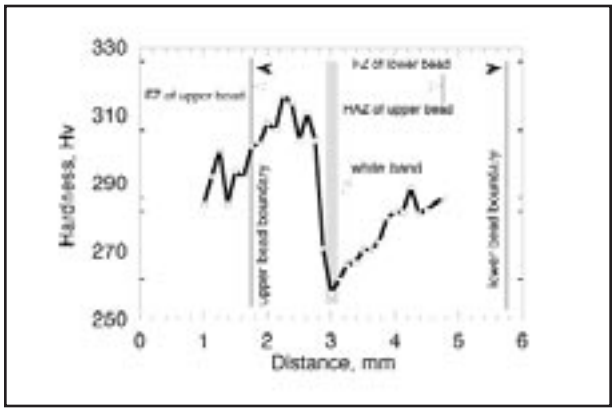

Fig. 2 — Hardness variation across the fusion boundary and heat affected zone within the weld metal of a weld bead in region 5 in Fig. 1C. In this plot, the "upper bead" was deposited after and on top of the "lower bead."

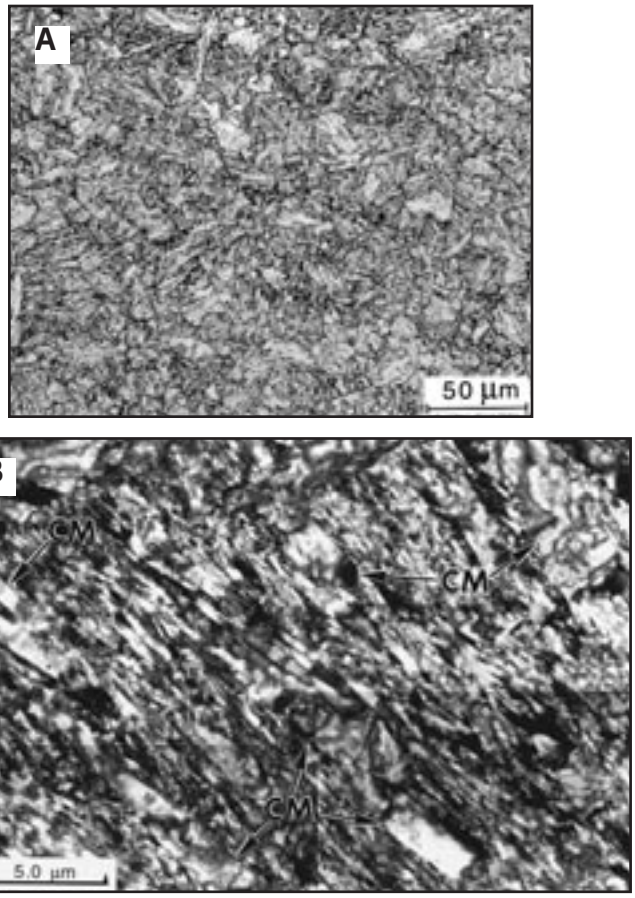

Fig. 3 — Tempered martensite microstructure of the unaffected HSLA-100 base metal. A — Light micrograph; B — TEM micrograph; arrows indicate some of the coarse martensite.

face, indentations were made at 1-mm spacing across a 59 x 28-mm area of the weldment. The data were then interpolated and converted into a color microhardness map using NCSA Image and Datascope software on a Macintosh computer — Fig. 1B. In some regions more closely spaced microhardness measurements were made (again with a 1-kg load) to more clearly determine microhardness trends across certain features. These additional measurements were performed with a spacing of 0.25 mm along each of four parallel lines, with a 0.25-mm spacing between these lines. Indents from every other line were offset (parallel to the line direction) by 0.125-mm, relative to the adjacent lines. These microhardness data are thus presented in Fig. 2 as averaged data points every 0.125 mm parallel to the direction of the four lines, but avoid the potential interference that might accompany measurements in which the indents were actually 0.125 mm apart along a single line. Additionally, measurements taken at progressively further spacings than 0.25 mm showed no appreciable change in the microhardness values, indicating a negligible interaction between the indents.

To prepare TEM specimens, 3.0-mm-diameter cylindrical specimens were electro-discharge machined from selected regions of the weldment. Disks of 0.25-mm thickness were cut with a diamond saw from these cylinders, mechanically thinned to 0.05 mm, then slightly dimpled. These slices were then electropolished to perforation in a Fischione twin-jet electropolishing unit with a solution of 100 g of anhydrous sodium chromate in 500 mL of glacial acetic acid. The foils were electropolished at room temperature with a current of about 24 mA (55 V). TEM observations were performed on a Philips CM 30 operating at 300 kV.

For comparison, microhardness maps were also constructed for welds made with two other exploratory ULC filler metals: ARC100 and CTC-08. ARC100 was developed by ESAB (a welding consumable manufacturer) to meet the Navy's MIL-100S specifications (82–120 ksi yield strength); these are the same

specifications for which CTC-03 was developed. ESAB has worked in conjunction with Electric Boat Corporation and a U.S. Navy working group (Ref. 6) to commercialize this alloy. CTC-08 was developed by NCEMT to satisfy the Navy's higher strength weld specification, MIL-120S (102–123 ksi yield strength) (Ref. 16). The compositions of these consumables are also provided in Table 1. While the CTC03D-HSLA100 and ARC100-HY80 welds were prepared with a heat input of 30 kJ/in. (1200 kJ/m), the CTC08A-HSLA100 and CTC08C-HSLA100 welds were prepared with heat inputs of 55 kJ/in. (2200 kJ/m) and 110 kJ/in. (4300 kJ/m), respectively.

Results and Discussion

Microstructure-Microhardness Variations and Correlations Across Weldment CTC-03D

The low-magnification solidification structure and the microhardness map of the transverse cross section of the CTC-03D weldment are shown in Figs. 1A and 1B, respectively. A transparency of the color microhardness map (Fig. 1B) was overlaid onto the macrograph in Fig. 1A to directly correlate the microhardness variations to specific macroscopic features, including the individual weld beads, the bead heat-affected zones within the fusion zone (B-HAZs, where B stands for bead), the base metal heat-affected zone and the unaffected region of the base metal. This direct correlation between the macrostructure and the microhardness was then used to select regions of the weldment (Fig. 1C) for detailed microstructural analysis. These regions are discussed below.

The HSLA-100 base plate (region 8 in Fig. 1C) has a quench-and-tempered microstructure (Fig. 3), which consists primarily of fine-lath martensite and significant amounts of coarse martensite (Ref. 17). TEM shows both of these phases contain numerous small copper precipitates.

The base metal HAZ, region 3 in Fig. 1C, contains the hardest regions (340–360 HV) of the entire weldment — Fig. 1B. This high hardness is due to the higher carbon content of the base metal (Table 1) in combination with the relatively high cooling rate due to the heat sink provided by the base metal. Accordingly, the microstructure of this region is martensitic and consists of both a fine untempered lath martensite and a coarse autotempered martensite — Fig. 4. This coarse martensite is typically an order of magnitude wider than the fine-lath martensite and often exhibits a planar interface at one end. However, optical microscopy tends to underestimate the amount of coarse martensite in the sample due to the small size of some of these martensite plates. The hardest region within the HAZ is located about midway across the HAZ — Fig. 1B. This is contrary to predictions based on grain size arguments alone (Ref. 18), which suggest the hardness maximum should occur adjacent to the fusion zone boundary. One contributing factor is a significant amount of softer coarse autotempered martensite forms in the coarse-grained HAZ, which reduces the microhardness directly adjacent to the fusion boundary.

The overlaying procedure shows the white bands in the macrograph (Fig. 1A) are soft and appear even softer wherever multiple bands intersect. These white bands exhibit greater surface roughness than the surrounding areas and thus appear whiter when viewed with oblique lighting — Fig. 1. Each white band is curved, and is clearly associated with the heat-affected zone of the corresponding weld bead lying above it. However, it is not obvious from Fig. 1B precisely how the local microhardness varies in the vicinity of a white band. Thus, finer-scale microhardness measurements were made across the white band that passes through region 5 — Fig. 2. This figure shows the hardness variation traversing from the fusion zone of a weld bead (B-FZ), across the bead boundary and through the bead heat-affected zone in the weld metal. The hardness initially increases upon crossing the bead boundary from the B-FZ into the B-HAZ, then drops sharply to a minimum at the white band. After passing the white band, the hardness gradually increases up to the as-deposited B-FZ hardness of about 300 HV. It is thus clear that the white bands are the softest regions of the weldment.

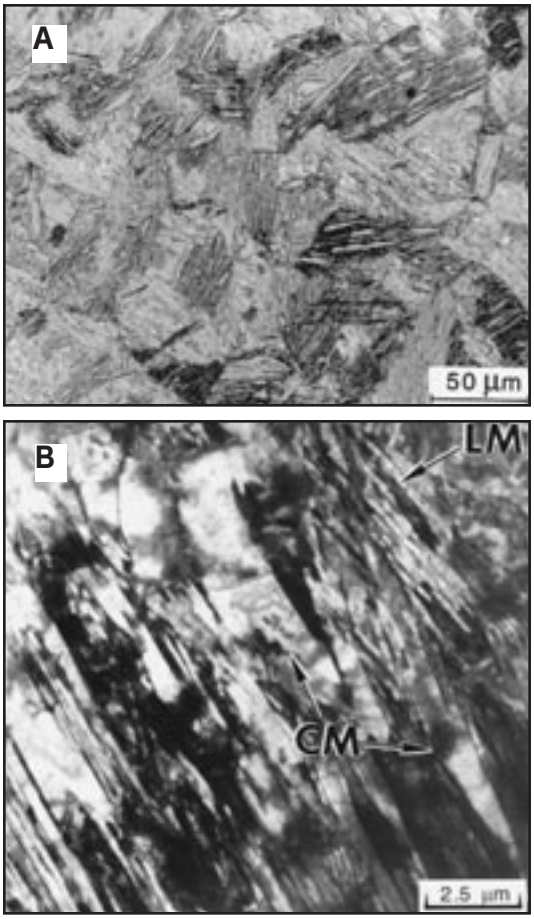

Fig. 4 — The HAZ microstructure of the base metal (region 3 in Fig. 1C). A — Light micrograph; B — TEM micrograph showing fine untempered lath martensite (LM) and coarse autotempered martensite (CM).

The largest soft region of the weldment, Region 1 in Fig. 1, is located in an area near where three white bands merge together. The microstructure of this region appears by optical microscopy (Fig. 5A) to consist of lath ferrite with some aligned ferrite laths at the grain boundaries. TEM observations (Fig. 5B) confirm that the microstructure is predominantly lath ferrite, with small amounts of retained austenite between the ferrite laths. This interlath-retained austenite often appears dark in TEM images (see arrow in Fig. 5B) and was identified by electron diffraction in this and other ULC weld metal investigations (Refs. 10, 22). Only minor amounts of martensite were observed in this region.

The predominance of ferrite at the white bands is caused by the low peak temperature and the relatively slow cooling rate at this distance from the bead boundary (Refs. 19, 20). As a result of heat flow from the bead deposited directly above this white band, this area was reheated and most likely experienced reaustenitizing within or directly above the intercritical range. The amount of ferrite may also have been enhanced by recalescence (increase in temperature caused by the liberation of the latent heat of transformation associated with the austenite-to-ferrite transformation) during cooling. Significant recalescence during cooling was observed in similar ULC alloys (Ref. 21) and ULC as-deposited weld metal (Ref. 22).

Region 2 is one of the hardest regions within the fusion zone. This region is in the last deposited weld bead, located at

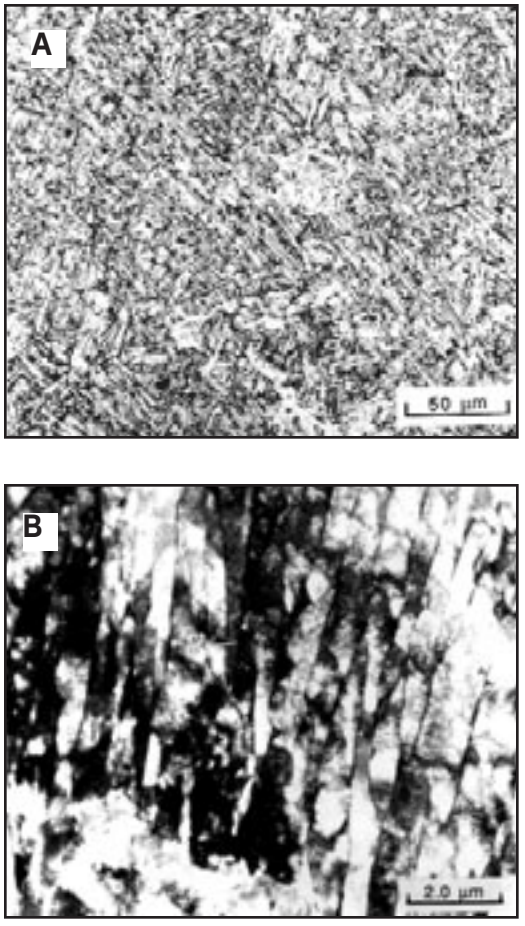

Fig. 5 — The microstructure of a large soft region in the fusion zone, in region 1 of Fig. 1C. A — Light micrograph; B — TEM micrograph of predominantly lath ferrite with some retained austenite (arrowed).

the top right of the weld in Fig. 1C. Since this is the last-deposited bead, the microstructure was not altered by subsequent bead deposition. Optical microscopy of Region 2 (Fig. 6A) reveals long laths of ferrite (up to more than 50 μm in length) within large prior austenite grains. TEM reveals the presence of significant amounts of fine-lath martensite between these large ferrite laths, as shown in Fig. 6B. This martensite is responsible for the high microhardness of this region. Optical microscopy often tends to overestimate the amount of ferrite in a microstructure when both ferrite and martensite are present in ULC steels (Ref. 10).

While no solid-state precipitates, such as carbides or carbonitrides, were ever observed in the ULC fusion zone, widely scattered spherical oxide inclusions (usually less than 1 μm in diameter) are present throughout the fusion zone — Figs. 6B, 7B. Energy-dispersive spectrometry reveals these inclusions to contain nearly equal amounts of manganese and titanium oxides in addition to small amounts of silicon oxide and aluminum oxide.

Region 4 (Fig. 1C) is one of the hardest regions of the fusion zone and lies within the root pass. The high microhardness of this region appears to be due to dilution from the backing plate in combination with the fast cooling rates from the backing plate and the base metal on either side of the V. Optical microscopy observations of Region 4 reveal a microstructure of acicular ferrite in a basket-weave morphology below the white band (Fig. 7A), while lath ferrite predominates above the white band. TEM observations (Fig. 7B) reveal the presence of isolated small packets of lath martensite within the acicular ferrite, contributing to the high hardness of this region.

Region 5 is a relatively hard region (330–340 HV) in the middle of the fusion zone — Fig. 1. This region, located between a bead boundary and its white band, appears somewhat similar to Region 1 in optical microstructure, except with finer features. The large ferrite laths observed in Regions 2 and 7 are not observed in this region. TEM observations instead reveal a majority of finer-lath ferrite with significant amounts of lath martensite.

Region 6, a soft region in the center of the fusion zone, is located below two adjacent bead boundaries — Fig. 1C. There appears to be no significant difference in microstructure between this area and Region 1 — Fig. 5. It consists mostly of aligned lath ferrite and possibly some lath martensite.

Region 7 lies in the B-HAZ of the last bead, about midway between the bead boundary and the white band — Fig. 1C. Both optical microscopy and TEM reveal a microstructure of long laths of ferrite very similar to that observed in Region 2 (Fig. 6B), with lath martensite and some fine-lath ferrite between the larger ferrite laths. The relatively fast cooling rate of this region produced a significant amount of lath martensite, resulting in the observed high hardness. The microhardness

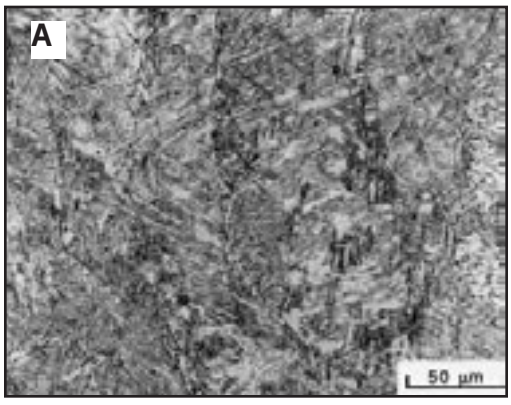

Fig. 6 — Microstructure of the fusion zone in region 2 of Fig. 1C. A — Light micrograph; B — TEM micrograph of relatively coarse laths of ferrite (F) within a lath martensite (LM) microstructure.

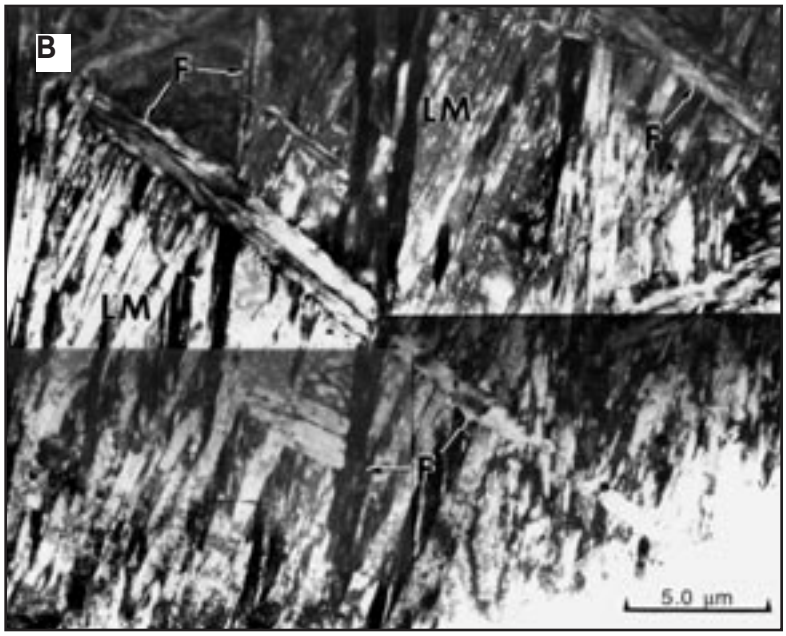

values in this region of the B-HAZ are slightly higher than those in the fusion zone of the bead, as shown in Fig. 2.

Comparison of Microhardness Maps from Welds Made with Different ULC Consumables

To compare the local property variations of welds made with different ULC filler metal candidates, the microhardness map of the weldment of HSLA-100 steel plate welded with the CTC-03 consumable (CTC-03D/HSLA-100) is compared in Fig. 8 with microhardness maps of welds made with other ULC consumables with various heat inputs. These weldments are identified as CTC-08A/HSLA-100, CTC-08C/HSLA-100, ARC-100/HY-80 and ARC-100/HSLA-100. The microhardness maps of the two CTC-08 welds (CTC-08A/HSLA-100 and CTC-08C/HSLA-100) were previously reported by Fonda, *et al.* (Ref. 10), while the microhardness maps of the two ARC-100 welds (ARC-100/HY-80 and ARC-100/HSLA-100) were constructed for the present study. In all five weldments, the hardest region is located in the HAZ about midway between the fusion zone boundary and the outer edge of the HAZ — Fig. 8. The weldments also show similar local hardness variations in the fusion zone — Fig. 8. The softest regions are located at the white bands, while the hardest regions are between those white bands and the weld bead boundaries.

CTC-03D vs. CTC-08A and CTC-08C

The CTC-08 welding consumable was designed to weld HSLA-100 steels, producing weldments that meet the MIL-120S specifications (Ref. 16). The CTC-08A and CTC-08C weldments shown in Fig. 8 were prepared by welding 1-in.-thick base plates of HSLA-100 with the CTC-08 consumable using heat inputs of 55 kJ/in. (2200 kJ/m) and 110 kJ/in. (4300 kJ/m), respectively. The fusion zone of the CTC-08C weld is clearly softer than that of the CTC-08A weld (Fig. 8), due to the higher heat input and resultant slower cooling rate of the CTC-08C weld, producing softer, ferritic microstructures. On the other hand, the HAZ hardnesses of these welds are comparable despite their differences in heat input.

Although the CTC-03 weldments satisfy the lower strength MIL-100S specification (Ref. 14) and the CTC-08 weldments meet the higher strength MIL-120S specification (Ref. 16), the fusion zone hardness of the CTC-03D weld is comparable to that of CTC-08A and actually exceeds that of CTC-08C. This is due to the high cooling rate of CTC-03D, despite its lean composition (Table 1). Nevertheless, CTC-03D exhibits weld metal cracking for high cooling rates (Refs. 23, 24). Therefore, the U.S. Navy shifted its emphasis onto a more promising ULC filler metal, designated ARC-100, which exhibits less susceptibility to weld metal cracking and better impact toughness at high cooling rates (Refs. 23, 24).

CTC-03D vs. ARC-100 on HY-80 or HSLA-100

ARC-100 was developed to meet the MIL-100S specification for welding of both HY and HSLA steels. Figure 8 shows a comparison between 2-in. -thick (50-mm)weldments of these two base plates welded with ARC-100 at the same heat input (30 kJ/in.). Although the fusion zone of the ARC-100/HY-80 weldment is very similar to the ARC-100/HSLA-100 weldment overall, the HAZ hardness of the HY-80 weldment is much higher (about 410 HV) than that of the HSLA-100 weldment (about 320 HV), as anticipated due to the higher carbon content of HY-80 — Table 1. This comparison provides a quantitative example of the benefits of the HSLA base plate over HY-80 steel plate. Even at a low heat input (30 kJ/in.) and without preheat, the HAZ of the higher strength HSLA-100 has lower hardness than that of lower strength HY-80. Therefore, the HSLA-100 HAZ should be much less susceptible to hydrogen-assisted cracking than the HY-80 HAZ. Nevertheless, the potential for hydrogen-assisted cracking in the HSLA-100 HAZ should still be considered due to its high hardness.

The ARC-100/HSLA-100 fusion zone is softer than that of CTC-03D, reflecting their compositional differences. For this double-V weld configuration, the root pass region of the ARC-100/HSLA-100 weld is harder than the surrounding area of the fusion zone, as shown in Fig. 8E. The higher hardness of this region is attributed both to dilution from the base plate and to the use of a compositionally rich flux coated consumable (MIL-10718-M) for the first two passes. Fast cooling rates due to the large heat sink of that area also contribute to the high hardness in this region. It is obvious from the microhardness map the fusion zone is lower in hardness than the HSLA-100 base plate (undermatched), even for the low 30 kJ/in. heat input used. This suggests even lower heat inputs might be considered, increasing the fusion zone hardness and matching with the unaffected base plate hardness. However, a further reduction in heat input might further elevate the already high hardness of the HAZ and increase the HAZ susceptibility to hydrogen-assisted cracking.

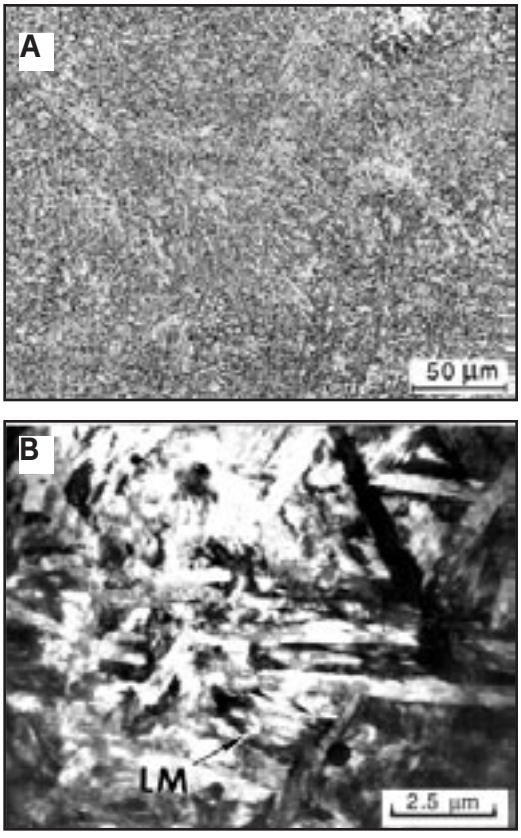

Fig. 7 — Microstructure from the hardest area within the root pass, region 4 in Fig. 1C. A — Light micrograph; B — TEM micrograph showing acicular ferrite with a small packet of lath martensite (LM).

Summary

Microstructure and microhardness variations have been investigated and correlated in an HSLA-100 steel weldment fabricated with an exploratory ultra-low-carbon (ULC) welding consumable designated CTC-03. These results are compared to the microhardness maps of four other weldments, made with different ULC candidate filler metals (designated CTC-08 and ARC-100), base plates and heat inputs. The principal findings from this investigation are summarized as follows:

1) A color microhardness mapping method in conjunction with detailed transmission electron microscopy and optical microscopy from local regions across weldments enables the direct correlation of microhardness variations to the corresponding microstructures.

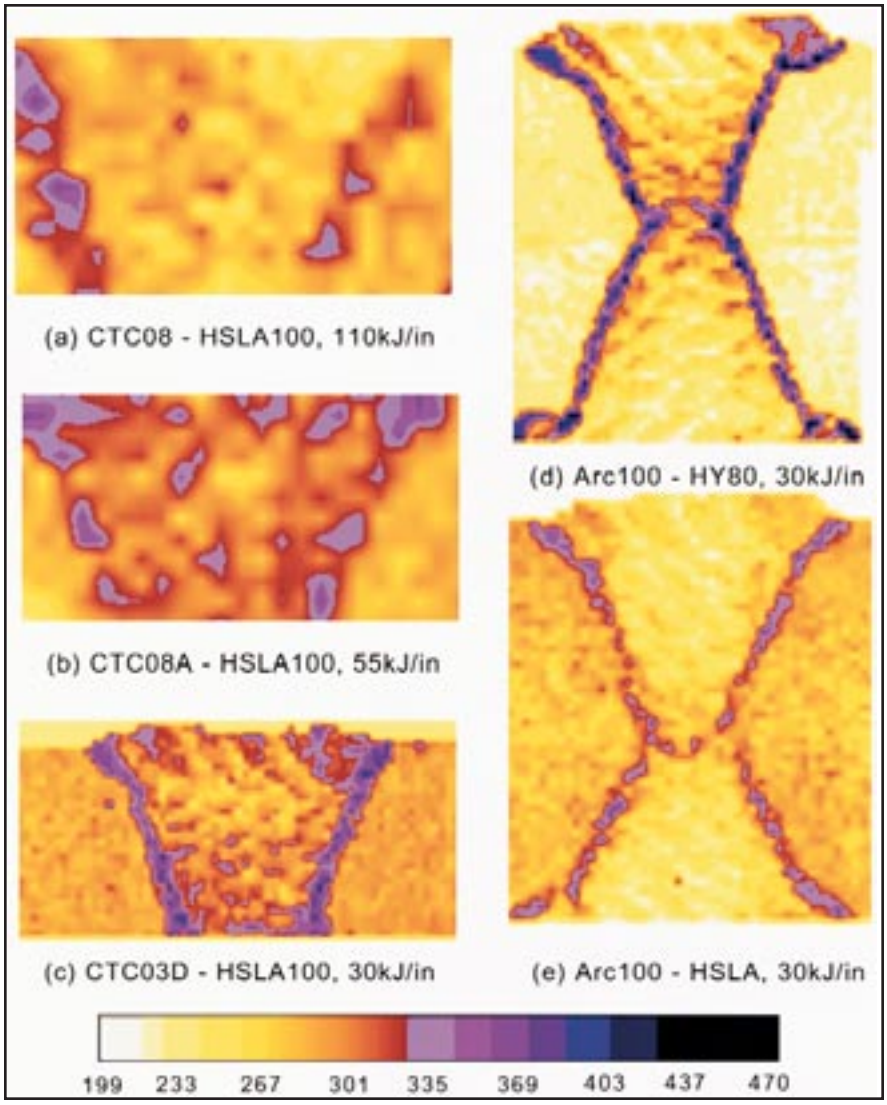

Fig. 8 — Microhardness maps of welds made with three different filler metals and different welding parameters. The corresponding microhardness scale is included at the bottom of this figure.

2) The fusion zone consists predominantly of lath ferrite with varying amounts (depending on location) of untempered fine lath martensite, as well as small amounts of interlath retained austenite and oxide inclusions. No polygonal ferrite or solid-state precipitates such as carbides or carbonitrides were observed in the fusion zone. The local variations in microhardness correlate well with the local variations in the microstructure.

3) The heat-affected zone of the base metal was the hardest region in each weldment examined, regardless of filler metal type, base metal or heat input. The hardness reaches a maximum about midway through the heat-affected zone of each weldment studied, rather than adjacent to the fusion boundary. In the CTC-03D weldment, the HAZ microstructure consists predominantly of untempered lath martensite, which is potentially susceptible to hydrogen cracking. The hardness decreases toward the fusion zone, where significant amounts of autotempered coarse martensite are also observed. Although the potential for failure is much worse for the HAZ of the HY-80 weldment, the hardness of the HSLA-100 HAZ remains significantly high. The microstructure and properties of the base metal HAZ, therefore, still deserve attention, aside from the improved fusion zone properties resulting from new ULC filler metals.

4) The softest regions in the fusion zone are in (and just outside) the curved white bands observed by low-magnification optical microscopy. The microstructure within these white bands consists predominantly of lath ferrite and aligned grain boundary ferrite, with small amounts of retained austenite.

5) In the vicinity of a weld bead, the hardness increases upon crossing the weld bead boundary into the bead heat-affected zone within the weld metal, then falls sharply to its lowest value at the white band. The hardness then gradually increases again up to that exhibited by the untempered microstructure of the next bead. The harder regions correspond to an increasing volume fraction of fine untempered lath martensite.

6) Despite the low heat input (30 kJ/in.), the fusion zone hardnesses of two of the new ultra-low-carbon filler metals, CTC-03D and ARC-100, are comparable to the base metal hardness. In fact, the low heat input of the CTC-03D weldment produced a fusion zone with a hardness comparable to that of the high heat input (but richer composition) CTC-08A weldment. However, when compared to the CTC-03 filler metal, the ARC-100 filler metal exhibits better impact toughness and better resistance to weld metal cracking at high cooling rates.

Acknowledgments

The authors would like to acknowledge funding through the Office of Naval Research (George Yoder, program manager) under contract 96PR04294-00. We acknowledge many helpful discussions with Paul Konkol and coworkers at NCEMT and Neil Fichtelberg of EB. We also appreciate the leadership of and helpful discussions with the managers of the Navy's Ultra Low Carbon Weld Consumable Development Program, John Deloach of NSWC-CD (technical manager) and Charles Null of NAVSEA (technical sponsor). We would particularly like to acknowledge the frequent assistance of Ed Pierpoint with many aspects of this research.

References

1. Holsberg, P. W., Gudas, J. P., and Caplan, I. L. 1989. Metallurgical design and processes in the U.S. Navy high strength steel welding. *Recent Trends in Welding Science and Technology* TWR'89, edited by S. A. David and J. M. Vitek, p. 593.

2. Flax, R. W., Keith, R. E., and Randall, M. D. 1971. *Welding the HY Steels*. ASTM Special Technical Publication 494, p.13.

3. Losz, I. M. B., and Challenger, K. D. 1989. Microstructure and properties of a copper-precipitation strengthened HSLA steel weldment. *Proceedings of the 2nd International Conference on Trends in Welding Research,* Gatlinburg, Tennessee, p. 229.

4. Czyryca, E. J., Link, R. E., Wong, R. J., Aylor, D. A., Montemarano,T. W., and Gudas, J. P. 1990. Development and certification of HSLA-100 steel for naval ship construction.

Naval Engineers Journal, 102(3): 63.

5. Cullison, A. 1994. Two paths, one goal: a consumable to weld HSLA100. *Welding Journal* 73(1): 51.

6. DeLoach, Jr., J. J. 1995. An overview of the U.S. Navy filler metal development program. *Proceedings of a TMS Symposium on Welding and Weld Automation in Shipbuilding*, edited by R. DeNale, Cleveland, Ohio, p. 85.

7. Holsberg, P. W., Guda, J. P., and Caplan, I. L. 1995. Navy's welding research picks up steam. *Advanced Materials and Processes* 138(1): 45.

8. Sampath, S. K., Civis, S. K., Dong, H., Konkol, P. J., and Green, R. S. 1995. Evaluation of new performance electrodes for GMA welding of HSLA-100 steel. *Proceedings of the ASM International Symposium on High Strength Steels for Structural Applications*, p.180.

9. Irving, B. 1995. U.S. Navy maintains high interest in funding for welding research. *Welding Journal* 74 (3): 41.

10. Fonda, R. W., Spanos, G., and Vandermeer, R. A. 1995. Processing-microstructure-property relationships. *Proceedings of the 4th International Conference Trends in Welding Research*, Gatlinburg, Tenn., p. 277.

11. Spanos, G., Fonda, R. W., Vandermeer, R. A., and Matuszeski, A. 1995. Microstructural changes in HSLA steel thermally cycled to simulate the heat-affected zone during welding. *Metallurgical and Materials Transactions A*, vol. 26A, p. 3279.

12. Blackburn, J. M., Vassilaros, M., Brandemarte, A., Fox, A., and Franke, G. 1995. The Effects of thermal cycling on ULCB weld metal. *A Proceedings on Welding and Automation in Shipbuilding,* by Structural Materials Division of TMS, edited by R. DeNale, p.167.

13. Devletian, J. H., Signh, D., and Wood, W. E. 1995. Ultra low carbon bainitic weld metal for joining 65 to 100 ksi yield steels. *A proceedings on Welding and Automation in Shipbuilding*, by Structural Materials Division of TMS, edited by R. DeNale, p.151.

14. Konkol, P. J. 1997. *Commercialization of Advanced Welding Consumables for HSLA-80 and HSLA-100 Steels*, reported by National Center for Excellence in Metal Working Technology, in Johnstown, Pa.

15. Brewer, A. W., Erven, K. A., and Krauss, G. 1991. *Materials Characterization*, p. 53, 27.

16. MIL-E-23765/2E 1994. *Electrodes and Rods — Welding Bare, Solid, or Alloy Cored; and Fluxes, Low Alloy Steel*.

17. Fonda, R. W., Spanos, G., and Vandermeer, R. W. 1994. Observations of late martensite in a low carbon steel,. *Scripta Metallurgica* 3: 683.

18. Ion, J. C., Eastering, K. E., and Ashby, M. F. 1984. A second report on diagrams of microstructure and hardness for heat-affected zones in welds. *Acta Metallurgica* 32(11): 1949.

19. Davenport, E. S., and Aborn, R. H. 1936. *Metallurgical Aspects of the Welding of Steel*, presented at Annual Meeting of AWS, Cleveland, Ohio. A contribution from the Research Laboratory of United States Steel Corp.

20. Nippes, E.F. 1959. The weld heat-affected zone. *Welding Journal* 38(1): 1-s to 18-s.

21. Fonda, R. W., Vandermeer, R. A., and Spanos, G. 1998. *Continuous Cooling Transformation (CCT) Diagram for Advanced Navy Welding Consumables*. Naval Research Laboratory Report NRL/MR/6324-98-8185.

22. Fonda, R. W., and Spanos, G. 1999. Microstructural evolution in ultra-low carbon steel weldments — part I: controlled thermal cycling and CCT diagram of the weld metal. *Metallurgical Transactions A*, in press.

23. Konkol, P. 1998. Concurrent Technologies Corp., private communication.

24. Deloach, J. D., Null, C., Fiore, S., and Konkol, P. 1999. The right welding wire could help the U.S. Navy save millions. *Welding Journal* 78(6): 55.

Preparation of Manuscripts for Submission to the *Welding Journal* Research Supplement

All authors should address themselves to the following questions when writing papers for submission to the Welding Research Supplement:

- ◆ Why was the work done?
- ◆ What was done?
- ◆ What was found?
- ◆ What is the significance of your results?
- ◆ What are your most important conclusions?

With those questions in mind, most authors can logically organize their material along the following lines, using suitable headings and subheadings to divide the paper.

1) **Abstract.** A concise summary of the major elements of the presentation, not exceeding 200 words, to help the reader decide if the information is for him or her.

2) **Introduction.** A short statement giving relevant background, purpose and scope to help orient the reader. Do not duplicate the abstract.

3) **Experimental Procedure, Materials, Equipment.**

4) **Results, Discussion.** The facts or data obtained and their evaluation.

5) **Conclusion.** An evaluation and interpretation of your results. Most often, this is what the readers remember.

6) **Acknowledgment, References and Appendix.**

Keep in mind that proper use of terms, abbreviations and symbols are important considerations in processing a manuscript for publication. For welding terminology, the *Welding Journal* adheres to ANSI/AWS A3.0-94, *Standard Welding Terms and Definitions.*

Papers submitted for consideration in the Welding Research Supplement are required to undergo Peer Review before acceptance for publication. Submit an original and one copy (double-spaced, with 1-in. margins on 8 1/2 x 11-in. or A4 paper) of the manuscript. Submit the abstract only on a computer disk. The preferred format is from any Macintosh® word processor on a 3.5-in. double- or high-density disk. Other acceptable formats include ASCII text, Windows™ or DOS. A manuscript submission form should accompany the manuscript.

Tables and figures should be separate from the manuscript copy and only high-quality figures will be published. Figures should be original line art or glossy photos. Special instructions are required if figures are submitted by electronic means. To receive complete instructions and the manuscript submission form, please contact the Peer Review Coordinator, Doreen Kubish, at (305) 443-9353, ext. 275; FAX 305-443-7404; or write to the American Welding Society, 550 NW LeJeune Rd., Miami, FL 33126.